Journal of Materials Chemistry A

Accepted Manuscript

ROYAL SOCIETY OF CHEMISTRY

www.rsc.org/materialsA

Multi-Layered Pt/Ni Nanotube Arrays with Enhanced Catalytic Performance for Methanol Electrooxidation

Sheng-Hua Ye, Jin-Xian Feng, An-Liang Wang, Han Xu and Gao-Ren Li*

MOE Laboratory of Bioinorganic and Synthetic Chemistry, KLGHEI of Environment and Energy Chemistry, School of Chemistry and Chemical Engineering, Sun Yat-sen University, Guangzhou 510275, China

E-mail: ligaoren@mail.sysu.edu.cn

Abstract

Novel Pt/Ni multi-layered nanotubes arrays (MLNTAs) are synthesized by the template-assisted layer-by-layer electrodeposition. The unique multi-layered structures in nanotube walls provide a new method to study the effects of heterointerfaces and structures on methanol electrooxidation. For the fabricated Pt/Ni MLNTAs, especially Ni@Pt@Ni@Pt NTAs, we observe obvious enhancements in the catalytic activity and durability compared with the monometallic Pt nanotube arrays (NTAs) and many Pt-based catalysts reported in literatures. Our synthesis approach presents a strategy to broaden heterointerfacial and structural effects in harnessing the true catalytic potential of Pt-based electrocatalysts and may lead to the wide applications for energy conversion and storage.

Keywords: multi-layered nanotube array, Pt/Ni, heterointerface, electrocatalyst, methanol oxidation

Introduction

Direct methanol fuel cell (DMFC) has been considered as a promising power source for portable electronic devices and electric vehicles.[1-3] Although great progress has been made towards non-Pt electrocatalysts, such as nanocrystalline $M_xMn_{3-x}O_4$ (M=divalent metals) spinels and the functionalized carbon nanotubes/graphenes, for oxygen reduction reaction (ORR) on cathode,[4-6] Pt still is the best electrocatalysts for methanol oxidation on anode and there is not yet better choice to replace Pt.[7-10] However, as the high cost and limited reserves of Pt, it is urgent to reduce the dosage of Pt used in the application process.

To date, one of the most successful techniques has involved partial substitution of Pt by a secondary metal. The Pt-based bimetallic catalysts with less consumption of Pt not only can inhere the properties of Pt constituent but also can display superior catalytic performance compared with their single metal counterparts because of synergistic effects between two metals.[11-17] Among various bimetallic catalysts, such as PtPd, PtAu, PtAg, PtCu, PtFe, and PtMn, the PtNi systems have received considerable attention because of their high catalytic activity and durability.[18-20] An alternative approach is to find proper nanostructures that can promote the reactivity of Pt-based catalysts. Recently, the Pt-based core/shell nanocrystals have been found to be promising catalysts because of much improved catalytic activity and durability.[21-23] The core/shell structure with Pt thin shell not only maximizes Pt exposure and minimizes Pt use for catalysis, but also offers the desired core-shell interactions to tune both electronic and surface strain effects for optimal catalysis,[21-23] indicating that the heterointerface plays an important role in improving the catalytic performance.

Our target in this study is the fabrication of multi-walled bimetallic nanotubes with alternating Pt/Ni multilayers for advanced electrocatalysts because one dimensional (1D) nanotubes have hollow

nanostructures and unique anisotropy and are less vulnerable to Ostwald ripening and aggregation during fuel cell operation.[24-25] The alternating Pt/Ni multilayer structures in the walls of nanotubes will bring rich abundant heterointerfaces. To further enhance catalytic performance of catalysts, forming porous walls for Pt/Ni nanotubes is another important goal because of the increase of accessible surface areas. This will let inner Pt and Ni layers can effectively take part in catalytic reactions. In this study, the above demands are well accomplished via the fabrication of Pt/Ni multi-layered nanotube arrays (MLNTAs) with porous structure by template-assisted layer-by-layer electrodeposition method. The heterointerfacial and structural effects of Pt/Ni MLNTAs were firstly exploited for methanol electrooxidation for DMFCs. The MLNTAs represent a novel prime example of electrocatalysts with well-defined multiple nanostructures, and they will provide rich heterointerfaces, high utilization rate, large surface area, and fast penetration/ diffusion of electroactive species. The electrochemical measurements demonstrated that the synthesized Pt/Ni MLNTAs exhibited much enhanced electrocatalytic activity and durability for methanol oxidation compared with monometallic Pt NTAs and many Pt-based catalysts and are promising electrocatalysts for DMFCs.

Experimental Section

Fabrication of ZnO nanorod arrays (NRAs) template. All chemical reagents were analytical grade. Electrodeposition was carried out in a simple two-electrode electrolytic cell via galvanostatic electrodeposition, and the graphite electrode was used as a counter electrode (spectral grade, 1.8 cm^2). The Ti plate (99.99%, 1.0 cm^2) was used as a working electrode, and it was prepared complying the following steps before each experiment: firstly polished by SiC abrasive paper from 300 to 800 grits, then dipped in HCl solution (5%) for 10 min and rinsed with acetone in ultrasonic bath for 5 min, and finally washed by distilled water. In the synthesis of ZnO NRAs, electrodeposition was carried out in 0.01 mol/L $Zn(NO_3)_2$ + 0.05 mol/L NH_4Cl solution at 0.4 mA/cm^2 at 70 ^{0}C for 1.5 h. SEM image of ZnO NRAs is

shown in Figure S1.

Synthesize of Pt/Ni MLNTAs: As illustrated in Scheme S1 and S2 in supporting information, the various Pt/Ni MLNTAs, such as Ni@Pt NTAs, Ni@Pt@Ni@Pt NTAs, Pt@Ni@Pt NTAs, and Pt@Ni@Pt@Ni@Pt NTAs were fabricated by using ZnO NRAs as templates. Electrodeposition of Pt layer was carried out in solution of 20 mM H_2PtCl_6 + 0.5 M NaCl + 2.5 mM sodium citrate for 20 min at 0.25 mA/cm^2. Electrodeposition of Ni layer was carried out in solution of 0.01 M $Ni(Ac)_2$ + 0.05 M H_3BO_3 + 0.05 M NH_4Cl for 20 min at 0.25 mA/cm^2. ZnO was removed by immersing the samples into $NH_3 \cdot H_2O$ solution (10%) for 3 h. Pt NTAs was fabricated by the electrodeposition of Pt layers on ZnO NRAs for 1h and its SEM image is shown in Figure S3.

Structural characterization: The morphologies of samples were characterized by field emission scanning electron microscopy (FE-SEM, JSM-6330F) and transmission electron microscopy (TEM, JEM-2010HR). Chemical-state analysis was determined by X-Ray photoelectron spectroscopy (XPS) using an ESCAKAB 250 X-Ray photoelectron spectrometer, all peaks corrected by C 1s line at 284.6eV as standard, and curve fitting and background subtraction were accomplished. Chemical component analysis was determined by inductively coupled plasma-atomic emission spectrometry (ICP-AES) using TJA IRIS(HR) spectrometer.

Electrochemical characterization: Electrochemical properties of the prepared electrocatalysts were studied in a standard three-electrode electrolytic cell. The Pt NTAs, Ni@Pt NTAs, Pt@Ni@Pt NTAs, Ni@Pt@Ni @Pt NTAs and Pt@Ni@Pt@Ni@Pt NTAs grown on Ti substrates served as the working electrodes. A Pt foil served as the counter electrode. A saturated calomel electrode (SCE) was used as the reference electrode. All potentials were the values vs SCE. Cyclic voltammetry (CV) and chronoamperometry were measured by a CHI660D electrochemical workstation (CH instruments, Inc.).

CV curves were recorded between -0.20 and 1.00 V *vs* SCE at 50 mV/s. Chronoamperometry curve for methanol oxidation was recorded at 0.65 V. For CV and chronoamperometry measurements of methanol oxidation reactions, an aqueous solution of 0.5 M H_2SO_4+0.5 M CH_3OH was utilized. All of the electrolyte solutions were purged with high purity N_2 for 10 min, and all of the electrochemical measurements were carried out at room temperature.

Results and Discussion

The details of the fabrication of Pt/Ni MLNTAs are described in the Experimental Section and Supporting Information. SEM images of Ni@Pt NTAs, Pt@Ni@Pt NTAs, Ni@Pt@Ni@Pt NTAs and Pt@Ni@Pt@Ni@Pt NTAs are shown in Figure 1a, 1e, 1i, 1m, respectively, which all shows the nanotubes have lengths of about 2 μm and are separate from each other. To prove the hollow structures, TEM images of the Ni@Pt NTAs, Pt@Ni@Pt NTAs, Ni@Pt@Ni@Pt NTAs and Pt@Ni@Pt@Ni@Pt NTAs are measured and are shown in Figure 1b, 1f, 1j, 1n, respectively, which show the above different NTAs were fabricated and they are porous structures. To prove the multi-layered structures in nanotubes, the elemental line-profile analysis was performed. For Ni@Pt NTAs, the elemental line-profile well demonstrates the double-layered Ni/Pt layers in the nanotube wall as shown in Figure 1d. The elemental line-profile of the Pt@Ni@Pt NTAs well proves three-layered Pt/Ni/Pt layers in the nanotube wall as shown in Figure 1h. The elemental line-profiles of Ni@Pt@Ni@Pt NTAs shown in Figure 1*l* and that of Pt@Ni@Pt@Ni@Pt NTAs shown in Figure 1*p* well prove that the nanotube walls are composed of four-layered Ni/Pt/Ni/Pt and five-layered Pt/Ni/Pt/Ni/Pt alternative layers, respectively.

To demonstrate the existence of Pt and Ni, the XPS spectra of samples were measured. Considering the same deposition conditions of Pt and Ni for various Pt-Ni samples in this study, the Ni@Pt NTAs were chosen as a representative to confirm the chemical state of Pt and Ni in the samples. Figure S5 shows the

XPS spectra of Ni@Pt NTAs in Pt *4f* and Ni *2p* regions. Each Pt *4f* peak can be deconvoluted into two pairs of doublets. A comparison of the relative areas of integrated intensity of Pt^0 and Pt^{II} shows that plentiful Pt exists as Pt^0 in the Ni@Pt NTAs, and only a small amount of Pt^{II} is observed. For the element Ni, each Ni *2p* peak is also deconvoluted into two pairs of doublets. The characteristic peaks at 855.9 and 873.6 eV correspond to Ni $2p_{3/2}$ and Ni $2p_{1/2}$ peaks of metallic Ni, respectively, confirming the presence of Ni^0 in the composite. In addition, two small shake-up peaks that are also the characteristic peaks of Ni were observed. Therefore, the above analysis suggests that the electrodeposition method used in this study can obtain the metallic Pt/Ni hybrid NTAs.

The Pt NTAs, Ni@Pt NTAs, Pt@Ni@Pt NTAs, Ni@Pt@Ni@Pt NTAs and Pt@Ni@Pt@Ni@Pt NTAs were firstly evaluated by the electrochemically active surface area (ECSA) that is an important parameter for the assessment of electrochemically active sites of catalysts. Figure 2a shows cyclic voltammograms (CVs) of Pt NTAs, Ni@Pt NTAs and Ni@Pt@Ni@Pt NTAs measured in N_2-purged 0.5 M H_2SO_4 solution at 50 mV/s. By using the charge passed for H-desorption (Q_H), the ECSA of Pt can be calculated using the following equation: $ECSA=Q_H/(0.21\times W_{Pt})$, where W_{Pt} represents the Pt loading (mg) in the electrode, Q_H represents the charge for H-desorption (mC/cm^2), and 0.21 represents the charge required to oxidize a monolayer of H_2 on clean Pt. The ECSA of Pt, Ni@Pt and Ni@Pt@Ni@Pt NTAs is calculated to be 29.7, 28.2, and 27.4 $m^2\cdot(g, Pt)^{-1}$, respectively. CVs of the Pt@Ni@Pt NTAs and Pt@Ni@Pt@Ni@Pt NTAs in N_2-purged 0.5 M H_2SO_4 solution at 50 mV/s are shown in Figure 2b, and the ECSA of Pt@Ni@Pt NTAs and Pt@Ni@Pt@Ni@Pt NTAs is calculated to be 34.6 and 31.6 $m^2\cdot(g, Pt)^{-1}$, respectively. The above ECSAs of various catalysts are comparable to that of PtNiP NTAs (28.4 $m^2\cdot(g, Pt)^{-1}$) reported in literature.[26]

To investigate the effect of heterointerface on catalytic activity, the cyclic voltammetry experiments of Pt NTAs, Ni@Pt NTAs and Ni@Pt@Ni@Pt NTAs were carried out in solution of 0.5 M CH_3OH +0.5 M

H_2SO_4, and the representative CVs are shown in Figure 3a. It is clearly seen that the mass peak current density of the Ni@Pt@Ni@Pt NTAs is 362.7mA/mg_{pt}, which is much higher than those of Ni@Pt NTAs (249.3 mA/mg_{pt}) and Pt NTAs (158.2 mA/mg_{pt}) (the current densities all are normalized to the mass of the Pt). Therefore, the Ni@Pt@Ni@Pt NTAs show an obviously enhanced mass electrocatalytic activity than Ni@Pt NTAs and Pt NTAs. Moreover, the mass peak current density of the Ni@Pt@Ni@Pt NTAs is also superior to those of Pt-based electrocatalyst as shown in Table S1. The high electrocatalytic activity of Ni@Pt@Ni@Pt NTAs can be attributed to rich Pt/Ni heterointerfaces. In addition, the Pt@Ni@Pt@Ni@Pt NTAs also show the much enhanced mass electrocatalytic activity compared with Pt@Ni@Pt NTAs and Pt NTAs as shown in Figure 3c. This also can be ascribed to the role of rich Pt/Ni heterointerfaces.

Chronoamperometry curves of the Pt NTAs, Ni@Pt NTAs and Ni@Pt@Ni@Pt NTAs were measured in solution of 0.5 M H_2SO_4 +0.5 M CH_3OH to evaluate the rate of surface poisoning (The potential was held at 0.65 V *vs* SCE) as shown in Figure 3b. It is obvious that the Ni@Pt@Ni@Pt NTAs exhibit a much slower current decay over time in comparison with the Ni@Pt NTAs and Pt NTAs, indicating a higher durability of the Ni@Pt@Ni@Pt NTAs. In addition, the Ni@Pt@Ni@Pt NTAs exhibit a higher mass current density than Ni@Pt NTAs and Pt NTAs, indicating that the Ni@Pt@Ni@Pt NTAs own a higher mass catalytic activity than Ni@Pt NTAs and Pt NTAs for methanol electrooxidation. In addition, the Pt@Ni@Pt@Ni@Pt NTAs also show much slower current decay over time and much higher mass current densities than Pt@Ni@Pt NTAs and Pt NTAs as shown in Figure 3d. Therefore, the above results demonstrate the important role of the Pt/Ni heterointerfaces in the Pt-Ni electrocatalysts for methanol oxidation. When the current densities all are normalized to the ECSA for above various Pt-Ni catalysts, the similar results were also obtained as shown in Figure S7.

In order to illustrate the interactions of heterointerfaces, XPS spectrum of Pt 4f and valence band spectrum of Pt were studied. Compared with Pt NTAs, the Ni@Pt NTAs, Pt@Ni@Pt NTAs,

Ni@Pt@Ni@Pt NTAs and Pt@Ni@Pt@Ni@Pt NTAs all show higher binding energy of Pt 4f peak (positive shift of ~0.5 eV) as shown in Figure 4a, suggesting the strong interactions between Pt and Ni layers.[26-28] However, Ni@Pt NTAs, Pt@Ni@Pt NTAs, Ni@Pt@Ni@Pt NTAs and Pt@Ni@Pt@Ni@Pt NTAs all show the almost same binding energy of Pt 4f peak, and the Pt 4f peaks are difficult to distinguish the effects of multiple heterointerfaces. As the limitation of XPS spectrum, the valence band spectra of Pt in Pt NTAs, Ni@Pt NTAs, Pt@Ni@Pt NTAs, Ni@Pt@Ni@Pt NTAs and Pt@Ni@Pt@Ni@Pt NTAs were measured as shown in Figure 4b. For Pt NTAs that have no heterointerface, there only is a constrictive peak locates at the binding energy of ~3 eV. With the increase of heterointerface number, the peak gradually becomes broader and broader. When the number of heterointerface increases to five, namely for Pt@Ni@Pt@Ni@Pt NTAs, two peaks clearly appear in valence band spectra of Pt as shown in Figure 4b(5). The above results well demonstrate electron interactions among the Pt/Ni heterointerfaces and well illustrate the change of binding energy of Pt valence electron with the increase of heterointerface number. Here the electron interactions among the heterointerfaces and the change of binding energy of Pt valence electron well interpret the effect of heterointerfaces on methanol electrooxidation.

Here we also find the structure of Pt-Ni MLNTAs is important for the performance of catalysts. The Ni@Pt NTAs showed better catalytic activity than Pt@Ni@Pt NTAs, and the Ni@Pt@Ni@Pt NTAs showed better catalytic activity than Pt@Ni@Pt@Ni@Pt NTAs as shown in Table S2. To investigate the role of interior Ni layers in the MLNTAs, the Ni@Pt NTAs and Pt@Ni@Pt NTAs were utilized as examples to study. XPS spectrum of the Ni@Pt NTAs before CV experiment was measured as shown in Figure 5a. The metallic Ni peaks were detected. In addition, two small shake-up peaks that are also the characteristic peaks of Ni were observed. Notably, after CV experiment, the Ni species almost all convert to NiOOH ($Ni^{3+}O^{2-}$) thoroughly as shown in Figure 5b, which is the stable phase in CH_3OH/H_2SO_4 solution.[29] Therefore, in the case of Ni@Pt NTAs, the $Ni^{3+}O^{2-}$ was produced after catalytic process. This

result suggests that the metallic Ni layers as interior walls of nanotubes will create $Ni^{3+}O^{2-}$ during the electrocatalytic process. However, for Pt@Ni@Pt NTAs, this phenomenon is not found. Recently, it has been reported that the $Ni^{3+}O^{2-}$ could be used as a catalyst for methanol electrooxidation, and Manoharan *et al* proposed the mechanism as follow:[30]

$$2Ni^{3+}O^{2-}+CH_3OH \rightarrow Ni^{2+}OH^{-}+Ni^{2+}O^{-}CH_2OH \rightarrow Ni^{3+}O^{2-}+Ni^{3+}O^{-}C^{-}HO +3H^{+} + e^{-} \quad (1)$$

$$Ni^{3+}O^{-}C^{-}HO \rightarrow Ni^{3+}O^{-}C^{-}=O+H^{+}+e^{-} \rightarrow Ni^{3+}O^{2-} + CO_2\uparrow + 2H^{+}+2e^{-} \quad (2)$$

Therefore, based on the above electrocatalytic mechanism, the existence of NiOOH ($Ni^{3+}O^{2-}$) during the electrocatalytic process can well account for better electrocatalytic activity of Ni@Pt NTAs than that of Pt@Ni@Pt NTAs. In addition, the better electrocatalytic activity of the Ni@Pt@Ni@Pt NTAs than the Pt@Ni@Pt@Ni@Pt NTAs also demonstrate the positive role of interior Ni layers in the MLNTAs. Therefore, among the various Pt NTAs, Ni@Pt NTAs, Pt@Ni@Pt NTAs, Ni@Pt@Ni@Pt NTAs and Pt@Ni@Pt@Ni@Pt NTAs, the Ni@Pt@Ni@Pt NTAs as catalysts show the most favorable structure and accordingly show the highest catalytic activity for methanol electrooxidation.

Conclusions

In summary, we have successfully fabricated the various Pt/Ni MLNTAs by template-assisted layer-by-layer electrodeposition at room temperature. The XPS results reported in this study well demonstrated electron interactions among the Pt/Ni heterointerfaces and well illustrated the change of binding energy of valence electron of Pt with the increase of heterointerface number. The bimetallic Pt/Ni MLNTAs, especially Ni@Pt@Ni@Pt NTAs, remarkably improved the catalytic activity and durability compared with monometallic Pt NTAs, demonstrating their promising potential as effective catalysts. The present encouraging findings might open up a new avenue in the development of high-performance bimetallic multi-layered nanotube array catalysts.

Ackonowledgements

This work was supported by National Natural Science Foundation of China (51173212 and J1103305), National Basic Research Program of China (2015CB932304), Natural Science Foundation of Guangdong Province (S2013020012833), Fundamental Research Fund for the Central Universities (13lgpy51), SRF for ROCS, SEM ([2012]1707), Project of High Level Talents in Higher School of Guangdong Province, Science and Technology Planning Project of Guangdong Province (2013B010403011) and Open-End Fund of Key Laboratory of Functional Inorganic Material Chemistry (Heilongjiang University), Ministry of Education.

References

1 M. Gao, Q. Gao, J. Jiang, C. Cui, W. Yao and S.-H. Yu, *Angew. Chem. Int. Ed.* 2011, **50**, 4905; b) X. Sun, D. Li, Y. Ding, W. Zhu, S. Guo, Z. Wang and S. Sun, *J. Am. Chem. Soc.* 2014, **136**, 5745.

2 a) H.-X. Liu, N. Tian, M. P. Brandon, Z.-Y. Zhou, J.-L. Lin, C. Hardacre, W.-F. Lin and S.-G. Sun, *ACS Catal.* 2012, **2**, 708; b) H.-H. Li, S. Zhao, M. Gong, C.-H. Cui, D. He, H.-W. Liang, L. Wu and S.-H. Yu, *Angew. Chem. Int. Ed.* 2013, **52**, 7472; c) N. Tian, Z.-Y. Zhou, S.-G. Sun, Y. Ding and Z. L. Wang, *Science* 2007, **316**, 732.

3 a) L. Wang and Y. Yamauchi, *J. Am. Chem. Soc.* 2013, **135**, 16762; b) C. Koenigsmann and S. S. Wong, *ACS Catal.* 2013, **3**, 2031; c) Y. Yamauchi, A. Tonegawa, M. Komatsu, H. Wang, L. Wang, Y. Nemoto, N. Suzuki and K. Kuroda, *J. Am. Chem. Soc.* 2012, **134**, 5100.

4 a) F. Cheng, J. Shen, B. Peng, Y. Pan, Z. Tao and J. Chen, *Nature Chem.* 2011, **3**, 79; b) Y. Li, P. Hasin and Y. Wu, *Adv. Mater.* 2010, **22**, 1926.

5 Y. Li, W. Zhou, H. Wang, L. Xie, Y. Liang, F. Wei, J.-C. Idrobo, S. J. Pennycook and H. Dai, *Nature Nanotechnol.* 2012, **7**, 394.

6 Y. Liang, Y. Li, H. Wang, J. Zhou, J. Wang, T. Regier and H. Dai, *Nature Mater.* 2011, **10**, 780.

7 a) H. Ataee-Esfahani, M. Imura and Y. Yamauchi, *Angew. Chem. Int. Ed.* 2013, **52**, 13611; b) C. Li, T. Sato and Y. Yamauchi, *Angew. Chem. Int. Ed.* 2013, **52**, 8050.

8 a) H. Wang, S. Ishihara, K. Ariga and Y. Yamauchi, *J. Am. Chem. Soc.* 2012, **134**, 10819; b) L. Zhang, N. Li, F. Gao, L. Hou and Z. Xu, *J. Am. Chem. Soc.* 2012, **134**, 11326.

9 a) L. Liu, E. Pippel, R. Scholz and U. Gösele, *Nano Lett.* 2009, **9**, 4352. (b) F. Shi, L. R. Baker, A. Hervier, G. A. Somorjai and K. Komvopoulos, *Nano Lett.* 2013, **13**, 4469.

10 S. W. Lee, S. Chen, W. Sheng, N. Yabuuchi, Y. Kim, T. Mitani, E. Vescovo and Y. Shao-Horn, *J. Am. Chem. Soc.* 2009, **131**, 15669.

11 a) C. Zhu, S. Guo and S. Dong, *Adv. Mater.* 2012, **24**, 2326; b) Y. Jia, Y. Jiang, J. Zhang, L. Zhang, Q. Chen, Z. Xie and L. Zheng, *J. Am. Chem. Soc.* 2014, **136**, 3748; c) J. Suntivich, Z. Xu, C. E. Carlton, J. Kim, B. Han, S. W. Lee, N. Bonnet, N. Marzari, L. F. Allard, H. A. Gasteiger, K. Hamad-Schifferli and Y. Shao-Horn, *J. Am. Chem. Soc.* 2013, **135**, 7985.

12 a) C. Xu, L. Wang, R. Wang, K. Wang, Y. Zhang, F. Tian and Y. Ding, *Adv. Mater.* 2009, **21**, 2165; b) R. Iyyamperumal, L. Zhang, G. Henkelman and R. M. Crooks, *J. Am. Chem. Soc.* 2013, **135**, 5521; c) Y. Kang, M. Li, Y. Cai, M. Cargnello, R. E. Diaz, T. R. Gordon, N. L. Wieder, R. R. Adzic, R. J. Gorte, E. A. Stach and C. B. Murray, *J. Am. Chem. Soc.* 2013, **135**, 2741.

13 a) Y. Kang, X. Ye, J. Chen, Y. Cai, R. E. Diaz, R. R. Adzic, Eric A. Stach and C. B. Murray, *J. Am. Chem. Soc.* 2013, **135**, 42; b) Q.-S. Chen, Z.-Y. Zhou, F. J. Vidal-Iglesias, J. Solla-Gullón, J. M. Feliu and S.-G. Sun, *J. Am. Chem. Soc.* 2011, **133**, 12930.

14 a) S. Jiang, Y. Ma, G. Jian, H. Tao, X. Wang, Y. Fan, Y. Lu, Z. Hu and Y. Chen, *Adv. Mater.* 2009, **21**, 4953; b) B. Y. Xia, H. B. Wu, X. Wang and X. W. Lou, *J. Am. Chem. Soc.* 2012, **134**, 13934; c) J. Wu, L. Qi, H. You, A. Gross, J. Li and H. Yang, *J. Am. Chem. Soc.* 2012, **134**, 11880.

15 a) S. Jiang, Y. Ma, G. Jian, H. Tao, X. Wang, Y. Fan, Y. Lu, Z. Hu and Y. Chen, *Adv. Mater.* 2009, **21**, 4953; b) Y. Yamauchi, A. Tonegawa, M. Komatsu, H. Wang, L. Wang, Y. Nemoto, N. Suzuki and K. Kuroda, *J. Am. Chem. Soc.* 2012, **134**, 5100.

16 a) H. Zhang, M. Jin, J. Wang, W. Li, P. H. Camargo, M. J. Kim, D. Yang, Z. Xie and Y. Xia, *J. Am. Chem. Soc.* 2011, **133**, 6078; b) C. Song, Y. Wang and N. L. Rosi, *Angew. Chem. Int. Ed.* 2013, **52**, 3993.

17 a) H. Yang, J. Zhang, K. Sun, S. Zou and J. Fang, *Angew. Chem. Int. Ed*. 2010, **49**, 6848; b) Z. Liu, G. S. Jackson and B. W. Eichhorn, *Angew. Chem. Int. Ed.* 2010, **49**, 3173.

18 C. Zhang, S. Y. Hwang, A. Trout and Z. Peng, *J. Am. Chem. Soc.* 2014, **136**, 7805.

19 a) X. Tuaev, S. Rudi, V. Petkov, A. Hoell and P. Strasser, *ACS Nano* 2013, **7**, 75674; b) S. Choi, S. Xie, M. Shao, J. Odell, N. Lu, H. Peng, L. Protsailo, S. Guerrero, J. Park, X. Xia, J. Wang, M. Kim and Y. Xia, *Nano Lett.* 2013, **13**, 3420.

20 X. Huang, E. Zhu, Y. Chen, Y. Li, C. Chiu, Y. Xu, Z. Lin, X. Duan and Y. Huang, *Adv. Mater.* 2013, **25**, 2974.

21 a) H. Yang, *Angew. Chem. Int. Ed*. 2011, **50**, 2674; b) K. Sasaki, H. Naohara, Y. Cai, Y. M. Choi, P. Liu, M. B. Vukmirovic, J. X. Wang and R. R. Adzic, *Angew. Chem. Int. Ed.* 2010, **49**, 8602.

22 a) J. Zhang, M. B. Vukmirovic, Y. Xu, M. Mavrikakis and R. R. Adzic, *Angew. Chem. Int. Ed.* 2005, **44**, 2132; b) J. Luo, L. Wang, D. Mott, P. N. Njoki, Y. Lin, T. He, Z. Xu, B. N. Wanjana, I.-I. S. Lim and C.-J. Zhong, *Adv. Mater.* 2008, **20**, 4342.

23 a) Z. Liu, G. Jackson and B. W. Eichhorn, *Angew. Chem. Int. Ed.* 2010, **49**, 3173; b) T. Ghosh, M. Vukmirovic, F. DiSalvo and R. R. Adzic, *J. Am. Chem. Soc.* 2010, **132**, 906.

24 a) S. Jiang, Y. Ma, G. Jian, H. Tao, X. Wang, Y. Fan, Y. Lu, Z. Hu and Y. Chen, *Adv. Mater.* 2009, **21**, 4953; b) H.-H. Li, C.-H. Cui, S. Zhao, H.-B. Yao, M.-R. Gao, F.-J. Fan and S.-H. Yu, *Adv. Energy Mater.* 2012, **2**, 1182.

25 a) W. Zhang, A. I. Minett, M. Gao, J. Zhao, J. M. Razal, G. G. Wallace, T. Romeo and J. Chen, *Adv. Energy Mater.* 2011, **1**, 671; b) L. Liu and E. Pippel, *Angew. Chem. Int. Ed.* 2011, **50**, 2729; c) S. Alia, G. Zhang, D. Kisailus, D. Li, S. Gu, K. Jensen and Y. Yan, *Adv. Funct. Mater.* 2010, **20**, 3742.

26 L. X. Ding, A. L. Wang, G. R. Li, Z. Q. Liu, W. Zhao, C. Y. Su and Y. X. Tong, *J. Am. Chem. Soc.* 2012, **134**, 5730.

27 A. L. Wang, H. Xu, J. X. Feng, L. X. Ding and Y. X. Tong. *J. Am. Chem. Soc.* 2013, **135**, 10703.

28 H. Xu, L. X. Ding, C. L. Liang, Y. X. Tong and G. R. Li. *NPG Asia Mater.* 2013, **5**, e69.

29 H. Bode, K. Dehmelt and J. Witte. *Electrochim. Acta* 1996, **11**, 1097.

30 R. Manoharan and J. B. Goodenough. *J. Marer. Chem.* 1992, **2**, 875.

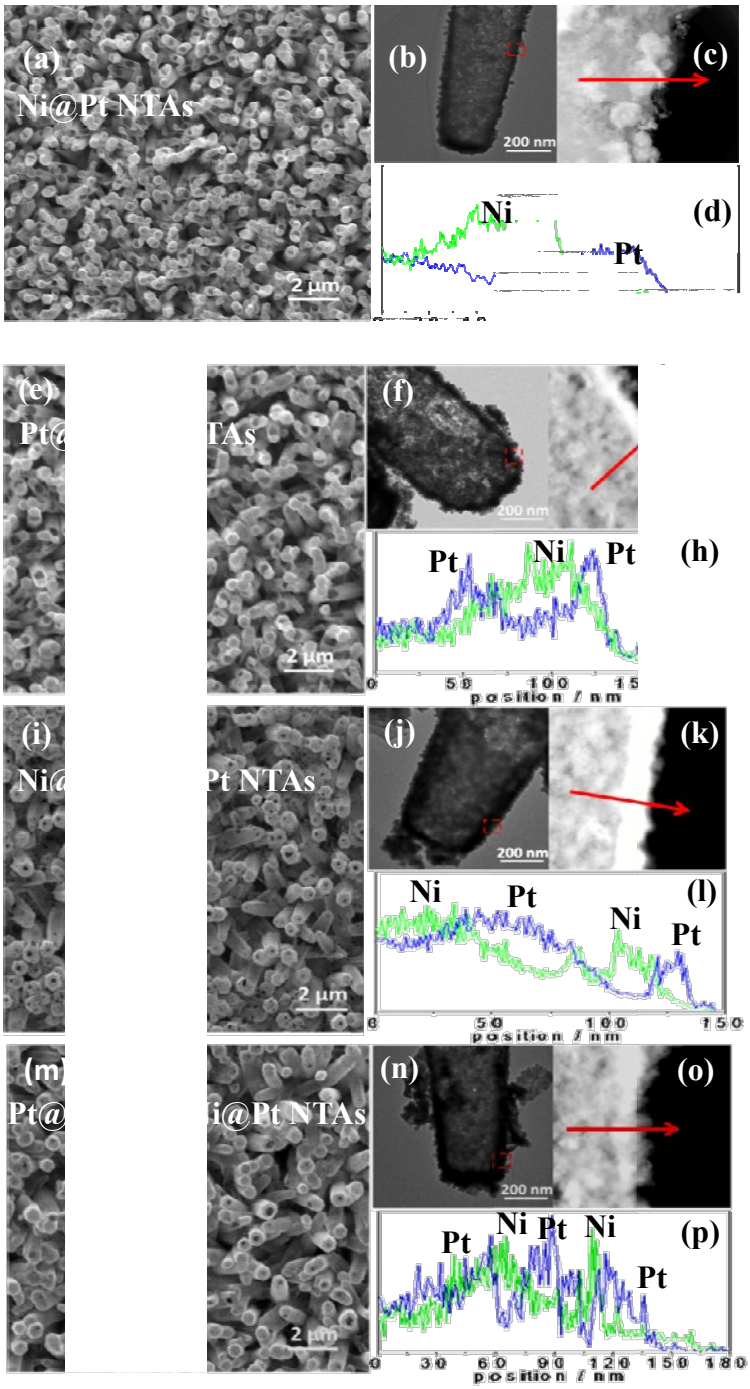

Figure 1. (a) SEM image, (b) TEM image, (c) nanotube wall, and (d) elemental line-profile of Ni@Pt NTAs; (e) SEM image, (f) TEM image, (g) nanotube wall, and (h) elemental line-profile of Pt@Ni@Pt NTAs; (i) SEM image, (j) TEM image, (k) nanotube wall, and (l) elemental line-profile of Ni@Pt@Ni@Pt NTAs; (m) SEM image, (n) TEM image, (o) nanotube wall, and (p) elemental line-profile of Pt@Ni@Pt@Ni@Pt NTAs.

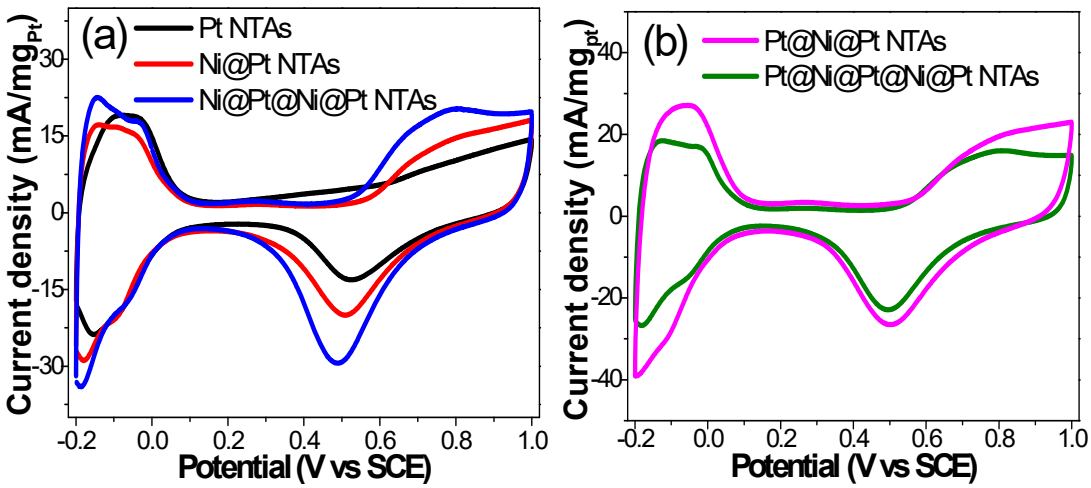

Figure 2. CVs of (a) Pt NTAs, Ni@Pt NTAs and Ni@Pt@Ni@Pt NTAs and CVs of (b) Pt@Ni@Pt NTAs and Pt@Ni@Pt@Ni@Pt NTAs in solution of 0.5 M H_2SO_4 at 50 mV/s.

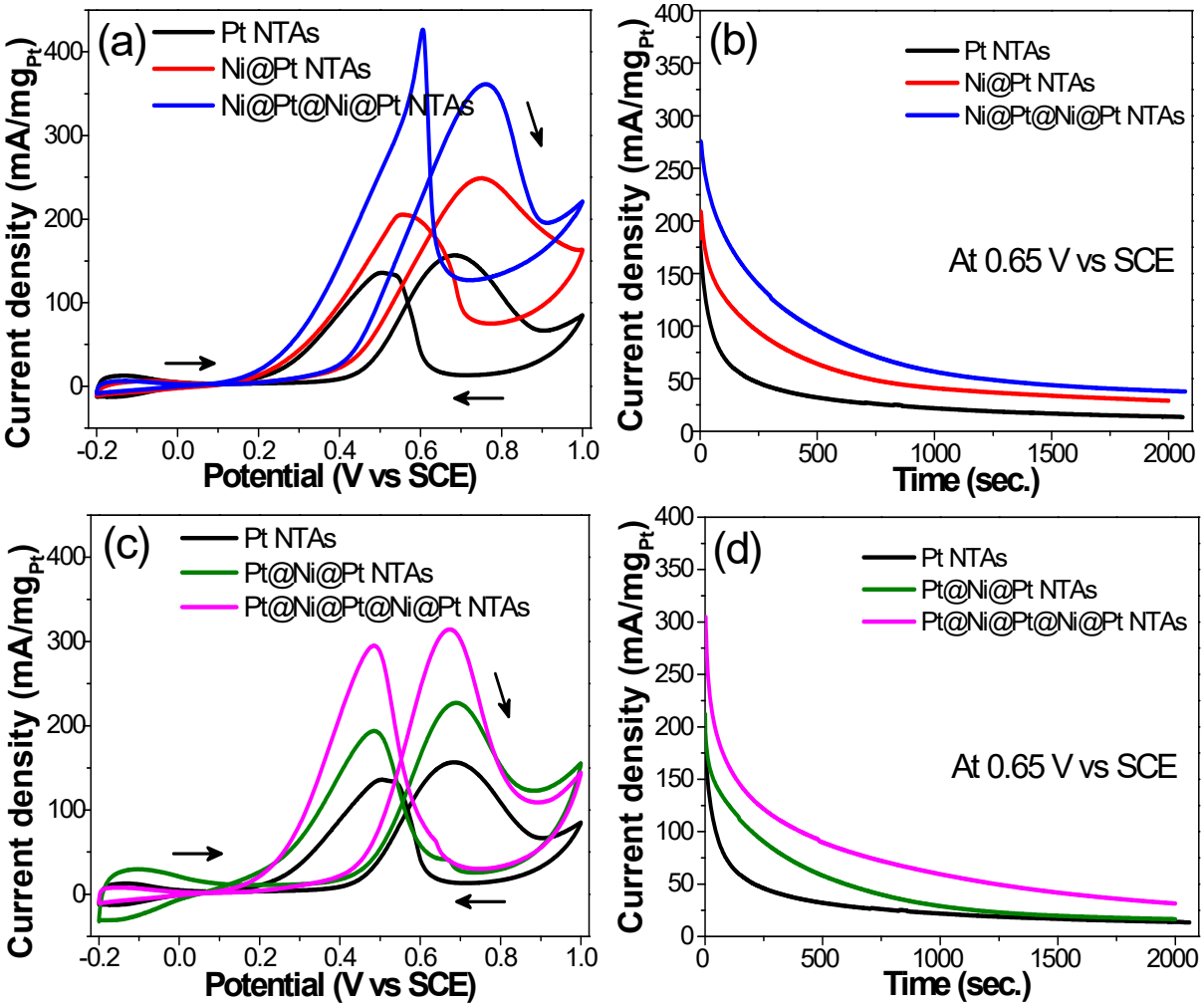

Figure 3. (a) CVs and (b) chronoamperometry curves of Pt NTAs, Ni@Pt NTAs and Ni@Pt@Ni@Pt NTAs in solution of 0.5 M H_2SO_4+0.5 M CH_3OH at 50 mV/s; (c) CVs and (d) chronoamperometry curves of Pt NTAs, Pt@Ni@Pt NTAs and Pt@Ni@Pt@Ni@Pt NTAs in solution of 0.5 M H_2SO_4+0.5 M CH_3OH at 50 mV/s (the current densities all are normalized to Pt loading).

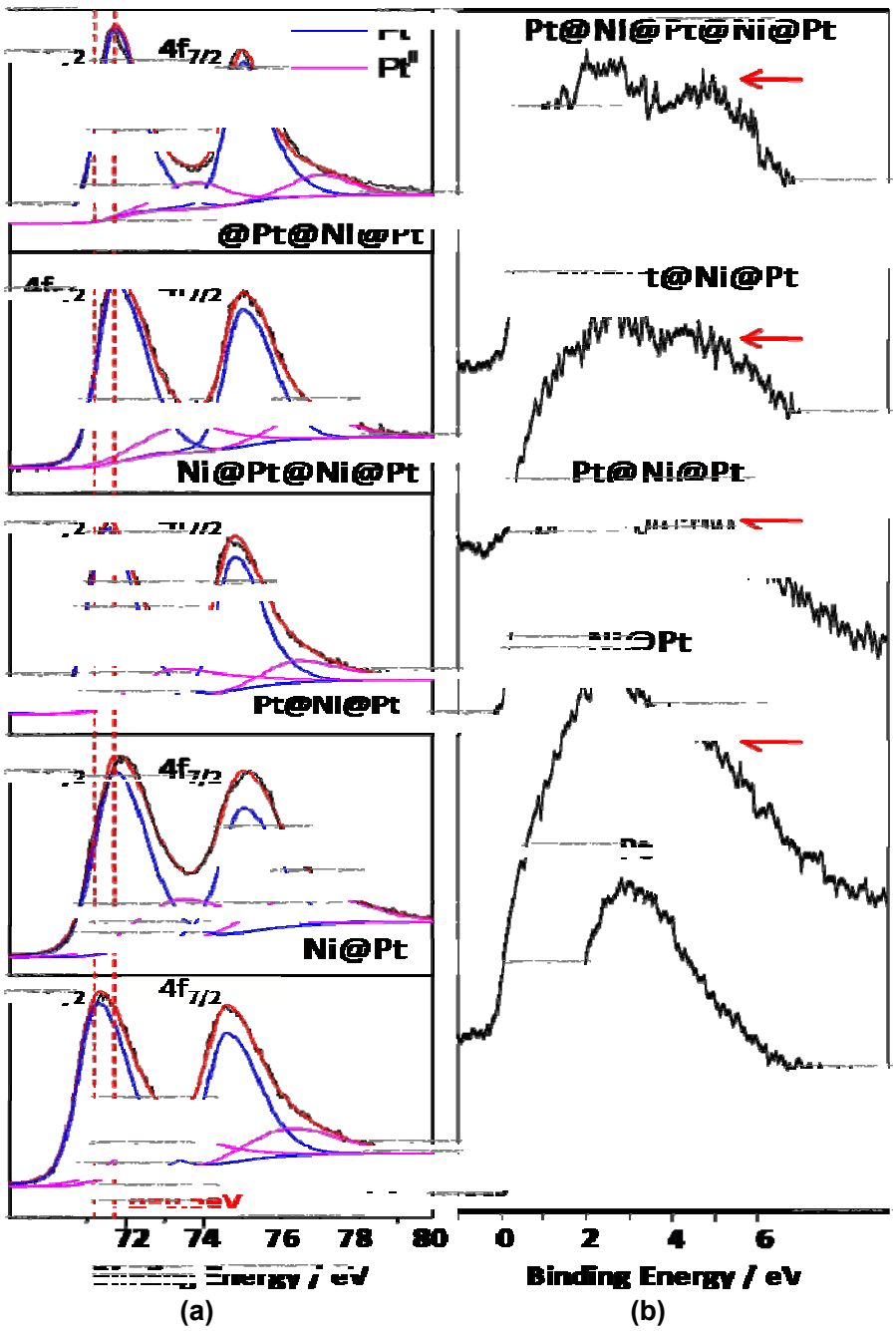

Figure 4. (a) XPS spectra and (b) valence band spectra of Pt in Pt NTAs, Ni@Pt NTAs, Pt@Ni@Pt NTAs, Ni@Pt@Ni@Pt NTAs and Pt@Ni@Pt@Ni@Pt NTAs.

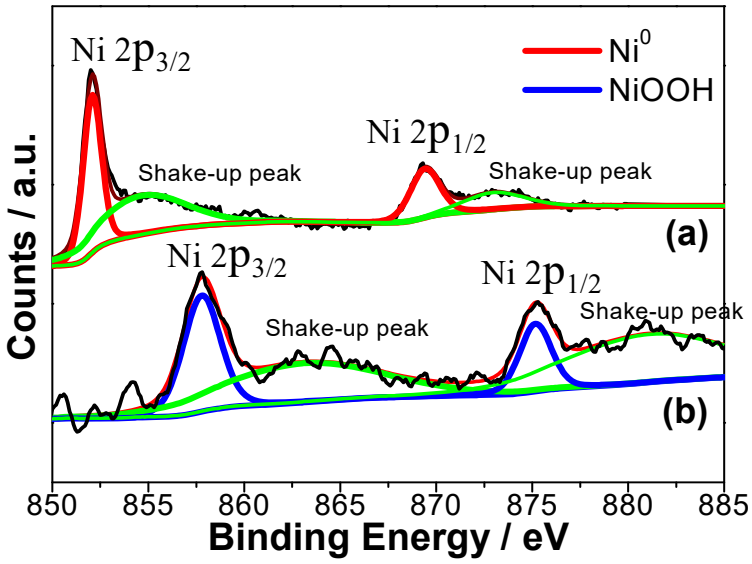

Figure 5. XPS spectra of Ni in the Ni@Pt NTAs (a) before and (b) after CV experiments.

Graphical Abstract Picture